Journal of Inorganic and General Chemistry
ZAAC
Zeitschrift für anorganische und allgemeine Chemie
www.zaac.wiley-vch.de
RESEARCH ARTICLE

DOI: 10.1002/zaac.202200152

Tetrazine Chelate Ligands Bridging Two [Ru(acac)$_2$] Fragments: Mixed Valency and Radical Complex Formation

Wolfgang Kaim,*[a] Isabell Löw,[a] Mark R. Ringenberg,[a] Brigitte Schwederski,[a] Vasileios Filippou,[a] and Jan Fiedler[b]

Dedicated to Thomas Schleid, Schoolmate and Colleague, on the Occasion of his 65th Birthday

Using bis(3-methyl-2-pyridyl)-1,2,4,5-tetrazine **1**, 3-(2-pyrimidyl)-6-methyl-1,2,4,5-tetrazine **2** and bis(2-pyrimidyl)-1,2,4,5-tetrazine = bmtz as ligands, the complexes **3** = [Ru(acac)$_2$(**1**)], **4** = {[Ru(acac)$_2$]$_2$(**1**)], **5** = {[Ru(acac)$_2$]$_2$(bmtz)], and **6** = {[Ru(acac)$_2$]$_2$(**2**)] were prepared and identified by structure analysis of crystallized material. The one-electron oxidized form **6**(PF$_6$) was also studied structurally, suggesting a Class II mixed-valent situation. The neutral dinuclear systems exhibit two reversible oxidation processes with comproportionation constants $10^{9.2} < K_c < 10^{14.1}$ and one reduction which were analyzed UV/vis/NIR and EPR spectroscopically. Oxidation produces largely metal-based mixed-valent cations with very weak intervalence absorptions in the near IR whereas the electron uptake occurs at the tetrazine acceptor.

Introduction

The peculiar heterocyclic structure of 1,2,4,5-tetrazines has received increasing attention recently as part of high-energy materials,[1] as component in bio-orthogonal chemistry,[2] and as part of electro- and photo-active materials.[3] The latter is based on the unusually low-lying LUMO of this electron-deficient ring containing four electronegative nitrogen atoms.[4] Within coordination chemistry the 1,2,4,5-tetrazine and its potentially chelating derivatives have served as two-step redox-active ligands with several metal binding sites and structure options.[4] Part of these structural options is the potential of tetrazines to bridge two[5,6] (or more[7,8]) metal centers by that π conjugated and potentially paramagnetic[8] mediator. Bridged metal-metal systems have also played a pivotal role in the study of intramolecular electron transfer leading to mixed-valent intermediates,[9–13] especially with the ruthenium(III,II) combination, of which the Creutz-Taube ion has been the most prominent example.[9,10]

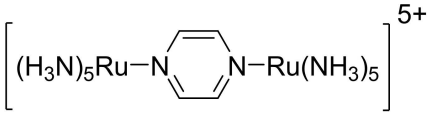

Creutz-Taube ion

Using three bis-chelating tetrazine derivatives (Figure 1) and the neutral, electron-rich[11–13] Ru(acac)$_2$ complex fragments (as opposed to [Ru(NH$_3$)$_4$]$^{2+}$[14] or [Ru(bpy)$_2$]$^{2+}$[15–18]) we have obtained the following compounds which were structurally characterized by X-ray diffraction in the solid and by spectroelectrochemistry (EPR, UV/Vis/NIR) in solution.[19–21]

3 = [Ru(acac)$_2$(**1**)],

4 = {[Ru(acac)$_2$]$_2$(**1**)],

5 = {[Ru(acac)$_2$]$_2$(bmtz)], bmtz = bis(2-pyrimidyl)-1,2,4,5-tetrazine, and

6 = {[Ru(acac)$_2$]$_2$(**2**)]

acac$^-$ = acetylacetonate = pentane-2,4-dionate

The latter was also crystallized in one-electron oxidized form **6**(PF$_6$) which allowed us to investigate the structural options of mixed-valency.

Results and Discussion

Ligand Presentation and Syntheses

The ligands **1** and **2** were obtained in the conventional way,[7] using appropriate organonitriles and hydrazine. Their analysis in the crystalline state (Tables S1-S5; Figures S1, S2) confirms the

[a] Prof. Dr. W. Kaim, Dr. I. Löw, Dr. M. R. Ringenberg, Dr. B. Schwederski, Dr. V. Filippou
Institut für Anorganische Chemie,
Universität Stuttgart,
Pfaffenwaldring 55, D-70550 Stuttgart, Germany
E-mail: kaim@iac.uni-stuttgart.de
[b] Dr. J. Fiedler
The Czech Academy of Sciences,
J. Heyrovský Institute of Physical Chemistry,
Dolejškova 3, 18223 Prague, Czech Republic

Supporting information for this article is available on the WWW under https://doi.org/10.1002/zaac.202200152

typical NN (1.33 Å) and CN bond lengths of the unreduced 1,2,4,5-tetrazine heterocycle.[4–6] Bmtz has been described before.[7] Torsional angles (ω) at the ring connections reflect steric repulsion, especially for **1** (ω = 37.2°) and will be discussed below in relation to the corresponding $Ru(acac)_2$ complexes.

The complexes **3–6** were obtained from the ligands and the Ru^{II} precursor $[Ru(acac)_2(MeCN)_2]$ as established for related examples.[13,19] Analytical and ^1H NMR data and the molecular structures of single crystals (Table S1) confirm the composition as detailed in the Introduction and below. In addition, the structural results provide information on isomerism, including *rac*/*meso* diastereomers (**4**-**6**),[17,18] configurational alternatives (**5**), and consequences of electron transfer (**6**, $\mathbf{6}^+$). The reaction with **1** yields mononuclear **3** and the *meso* form of dinuclear **4**. Whereas **5** was crystallized as the *meso* isomer from the *rac*/*meso* mixture, the reaction of $[Ru(acac)_2(MeCN)_2]$ with **2** yielded *rac* and *meso* diastereomers of **6** in addition to some mononuclear material.

Structure Discussion of Complexes

Compound ***3***. The mononuclear **3** (Δ and Λ enantiomers) exhibits the expected[11–21] chelation of $Ru(acac)_2$ by one N-(pyridyl) and one N(tetrazine) center (Figure 2, Tables 1, S1, S6, S7). The uncoordinated 3-methyl-2-pyridyl ring is twisted by 62.7° relative to the RuO_2N_2 plane, favoured by the repulsion of the methyl group and enhanced relative to the value of 37.2° for the free ligand. The NN[13] and short (N_{tz}) vs long (N_{py}) RuN distances (Table 1) suggest a moderate degree of π back donation from electron rich[11–13,19] $Ru(acac)_2$ to the π accepting tetrazine, however, a major metal-to-ligand electron transfer as

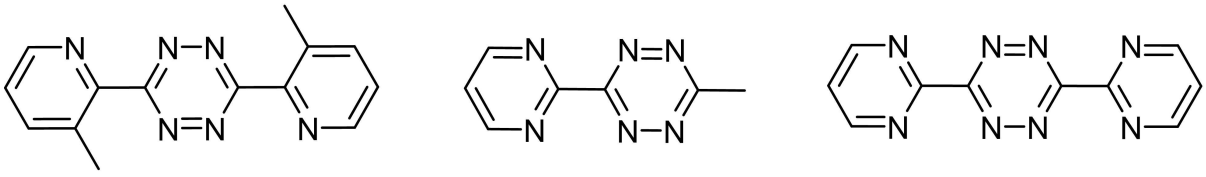

Figure 1. Tetrazine ligands bis(3-methyl-2-pyridyl)-1,2,4,5-tetrazine **1**, 3-(2-pyrimidyl)-6-methyl-1,2,4,5-tetrazine **2** and bis(2-pyrimidyl)-1,2,4,5-tetrazine, bmtz, used in this article.

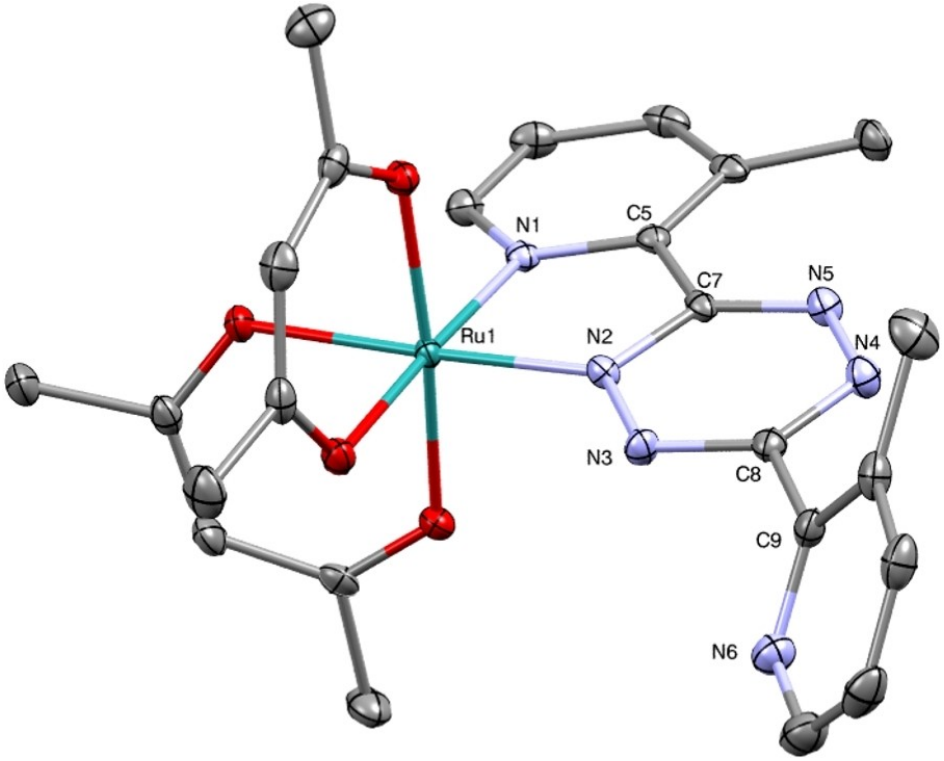

Figure 2. Molecular structure of **3** in the crystal of $\mathbf{3} \times CH_2Cl_2$. 50 % Probability, H atoms omitted for clarity.

Table 1. Selected bond lengths (Å) of complexes in the solid.

3×CH_2Cl_2	N2	N3	1.353(2)
	N4	N5	1.360(3)
	N1	Ru1	2.0240(17)
	N2	Ru1	1.9076(18)
4	N2	N3	1.358(8)
	N5	N6	1.349(8)
	Ru1	N1	2.030(6)
	Ru1	N2	1.933(6)
	Ru2	N4	2.020(6)
	Ru2	N5	1.941(6)
5	N3	N6	1.353(10)
	N4	N5	1.350(10)
	N3	Ru2	1.950(7)
	N1	Ru1	2.060(7)
	N2	Ru2	2.042(7)
	N4	Ru1	1.968(7)
6	N1	N2	1.388(10)
	N3	N4	1.371(10)
	N1	Ru1	1.954(8)
	N4	Ru2	1.941(7)
	N5	Ru2	2.039(8)
	N6	Ru1	2.035(7)
6(PF_6)	N3	N4	1.366(2)
	N5	N6	1.351(2)
	N3	Ru2	1.9370(17)
	N1	Rul	2.0631(16)
	N2	Ru2	2.0650(17)
	N6	Ru1	2.0448(17)

found for {[Ru(acac)$_2$]$_2$(μ-abpy)}, abpy = azo-2,2′-bispyridine,[13] cannot be deduced.

Compound ***4***. Dinuclear **4** is obtained as a single diastereomer which can be identified structurally as the *meso* form (Figure 3).[13] The NN and RuN bond parameters (Tables 1, S8, S9) are not very different from those of **3** or the bptz analogue (bptz = bis(2-pyridyl)-1,2,4,5-tetrazine).[12] The stronger back donation from the metals to the tetrazine ring is evident from the shortened Ru–N bonds (Table 1). The conformation for the central Ru-(μ-tetrazine)-Ru unit is largely planar with torsional angles $< 5°$.

Compound ***5***. Several configurational isomers (1,2-, 1,3- or 1,4-positioning) can be conceived for a dinuclear complex of the potentially tetrakis-chelating bmtz.[7,8] Compounds of higher nuclearity were not detected in spite of the stoichiometric ratio of 1:4 for the reaction. Instead of the perhaps expected inversion-symmetric 1,3-configuration

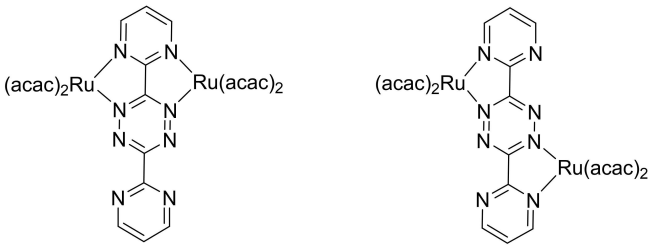

1,4 1,3

compound **5**

the alternative 1,4-arrangement with opposite Ru(acac)$_2$ groups was found (Tables 1, S10, S11; Figure 4), which exhibits a shorter metal-metal distance (5.424(2) Å) while maintaining small repulsion. The *meso* diasteromer has been established for the crystallized material although a further isomer was found by ^{1}H NMR spectroscopy. The free 2-pyrimidyl ring is twisted by 15.6(9)° in *meso*-**5** relative to the plane containg the ruthenium centers. The NN and RuN bond parameters (Table 1) are reflecting stronger π back donation to the tetrazine ring. The

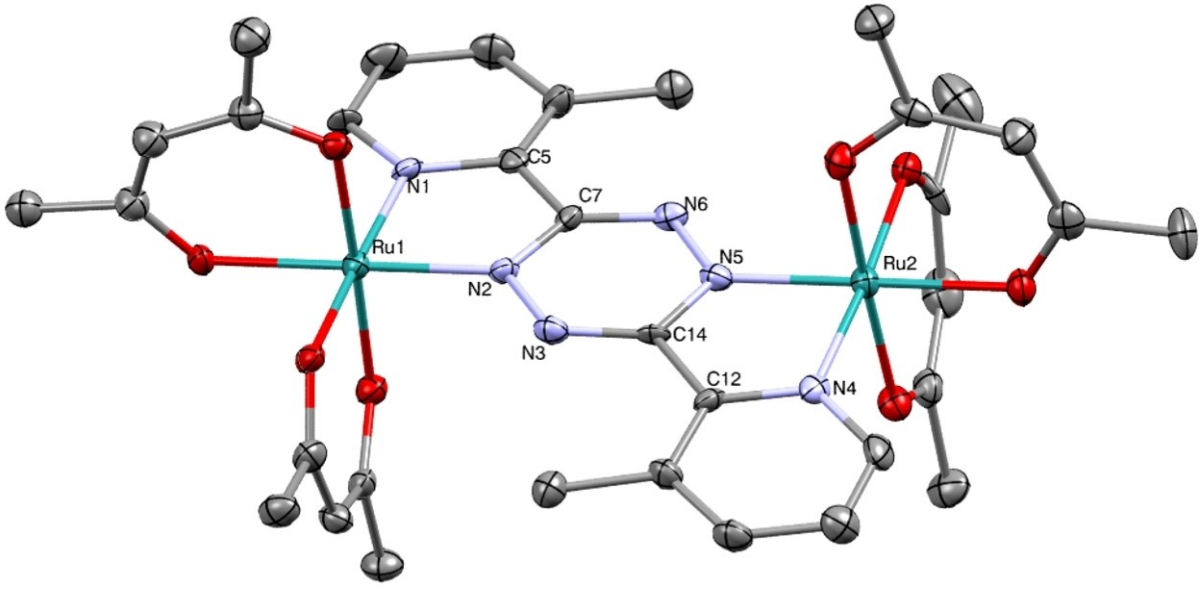

Figure 3. Molecular structure of *meso*-**4** in the crystal. 50 % Probability, H atoms omitted for clarity.

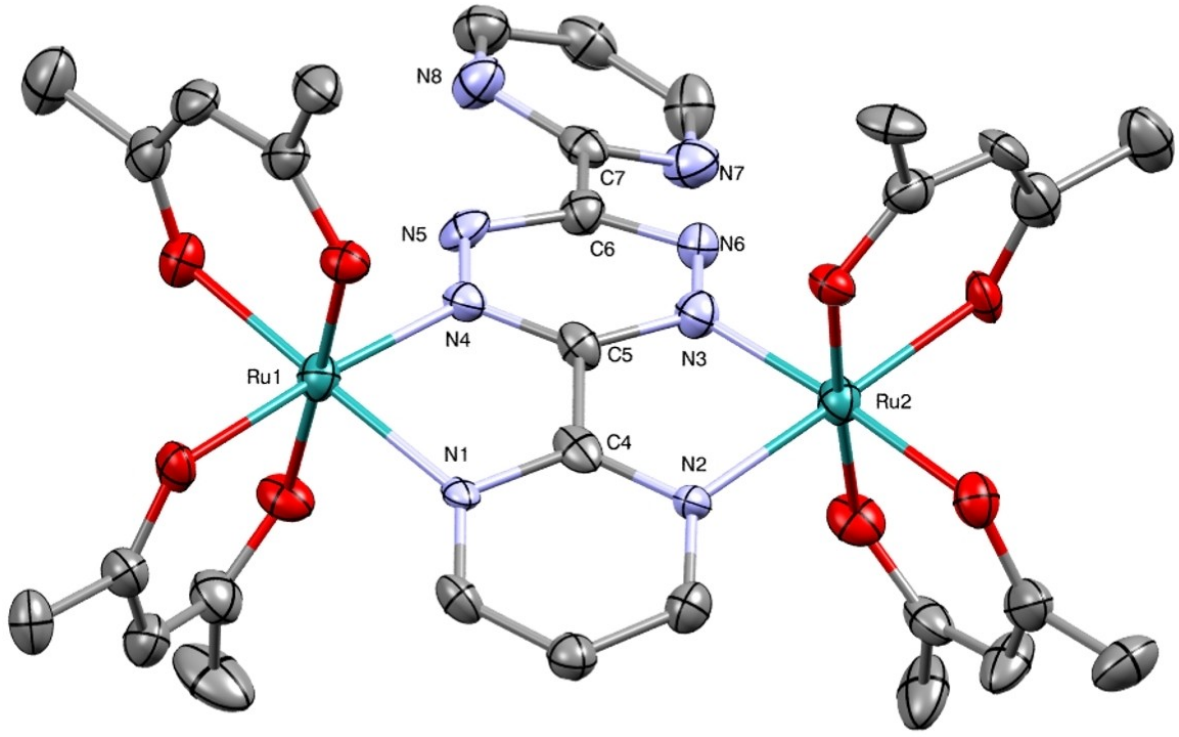

Figure 4. Molecular structure of *meso*-**5** in the crystal. 50 % Probability, H atoms omitted for clarity.

lengthening of the Ru-tetrazine bonds in dinuclear complexes may be due to the fact that the electron demand of the tetrazine ligand is satisfied by the presence of two donors instead of one.

Compound ***6***. The situation of *meso*-**5** is similarly observed for the *meso*-form of **6** without significant difference of the bond parameters (Tables 1, S12, S13; Figure 5). The RuN_{tz} bonds are typically shorter at 1.95 Å than the RuN_{pym} bonds of 2.04 Å (Table 1). Fortunately, it was also possible to crystallize the one-electron oxidized form as the *rac* diastereomer **6**(PF_6) from the reaction of *rac*/*meso* **6** with $AgPF_6$ (Tables 1, S14, S15; Figure 6). While the slight contraction of NN and RuN bonds (Table 1) on oxidation may be expected, the most significant result is the remarkable difference between the ruthenium-tetrazine bonds Ru2 N3 at 1.9370(17) Å and Ru1 N6 at 2.0448(17) Å (Table 1). This considerable disparity strongly suggests different oxidation states in the mixed-valent $\mathbf{6}^+$, corresponding to a Class II behavior[9,22] with the localized oxidation occurring on Ru1, in spite of the relatively short metal-metal distance of 5.431(3) Å.

A further notable result is the similarity of Ru2-N_{tz} distances for **6** (1.941(7) Å) and $\mathbf{6}^+$ (1.9370(17) Å).

Table 2. Half-wave potentials $E_{1/2}$, peak potential differences ΔE and comproportionation constants K_c (cations) of compounds.[a]

compound	$E_{1/2}$[b] (ΔE)[c]				
	Ox3	Ox2	Ox1	Red1	K_c[h]
1	–	–	–	−1.19 (90)	–
2	–	–	–	−1.26 (70)	–
bmtz[d]	–	–	–	−1.12[e]	–
3	–	–	0.13 (80)	−1.55 (120)	–
4	1.35[f]	0.48 (70)	−0.35 (70)	−1.76 (80)	$10^{14.1}$
5	1.51[f]	0.65 (120)	0.11 (100)	−1.31 (140)	$10^{9.2}$
6 *rac* or *meso*[g]	1.46[f]	0.56 (90)	−0.01 (80)	−1.50 (120)	$10^{9.7}$
6 *rac* or *meso*[g]	1.45[f]	0.54 (90)	−0.02 (80)	−1.51 (110)	$10^{9.5}$

[a] From cyclic voltammograms at room temperature in CH_2Cl_2/0.1 M Bu_4NPF_6, Pt, 100 mV/s scan rate. [b] In [V] vs. $[Fe(C_5H_5)_2]^{+/0}$. [c] ΔE ($=E_{pc}$-E_{pa}) in [mV]. [d] Au electrode. [e] Peak potential E_{pc} for irreversible process. [f] Peak potential E_{pa} for irreversible process. [g] Assignment not established. [h] log K_c (25 °C) $=(E_{ox2}-E_{ox1})/0.059$ V.

Cyclic voltammetry

Table 2 and Figures 7, S3-S5 show the results from electrochemical measurements in CH_2Cl_2/0.1 M Bu_4NPF_6. For the dinuclear compounds **4**–**6** reversible one-electron processes were observed for two oxidations and one reduction. The systems studied exhibit only small variation, caused by donor substituents as in **4** (shift to negative potentials) or acceptor substitution as in **5** (shift to positive potentials). Diastereoisomerism does not have a significant effect either (Figure 7).

As established by EPR (see below) the reduction occurs at the bridging ligands with unreduced tetrazine whereas the oxidation occurs stepwisely at the metals. The difference between the two oxidation potentials can be converted into an equilibrium constant $K_c = e^{nF\Delta E/RT} = [A^{\bullet+}]^2/[A][A^{2+}]$ for

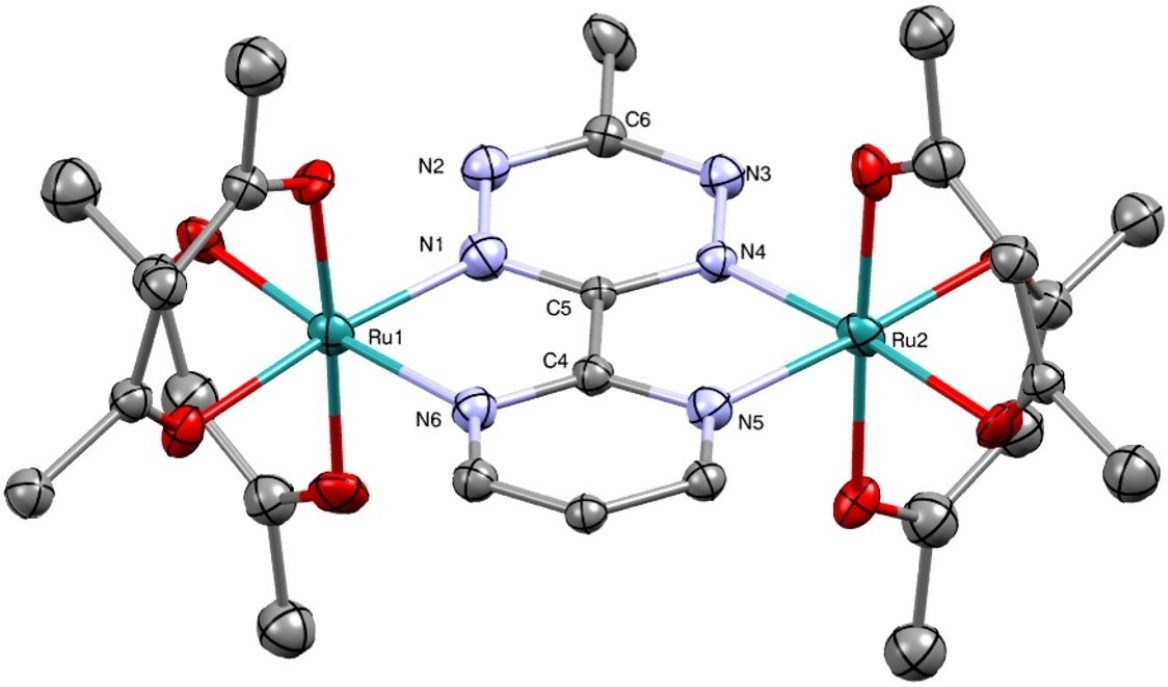

Figure 5. Molecular structure of *meso*-**6** in the crystal. 50 % Probability, H atoms omitted for clarity.

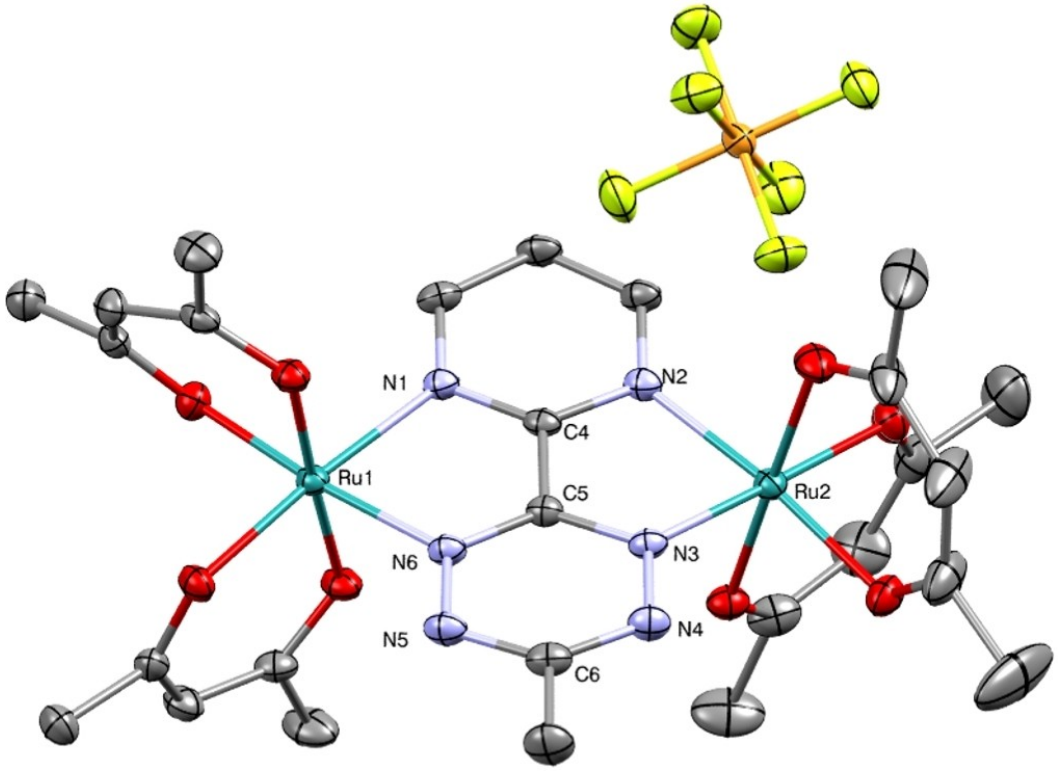

Figure 6. Molecular structure of *rac*-**6**(PF_6) in the crystal. 50 % Probability, H atoms omitted for clarity.

comproportionation,[9,10,18] which is one of the defining parameters for mixed-valent intermediates. The values obtained here (Table 2) of $10^{9.2}$–$10^{14.1}$ are typically[4,14,18] large; even the prototypical Creutz-Taube ion has only $K_c = 10^6$.[9]

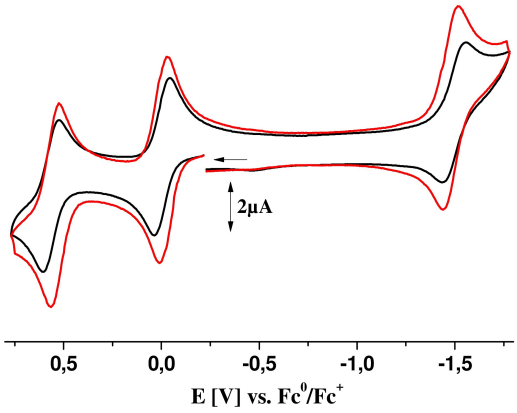

Figure 7. Cyclic voltammograms of the separated *rac* and *meso* diastereoisomers of **6** in CH_2Cl_2/0.1 M Bu_4NPF_6, Pt,100 mV/s scan rate.

EPR spectroscopy

In situ one-electron oxidation or reduction of the diamagnetic precursor compounds **3**–**6** yields EPR signals which can serve to identify the site of electron transfer. Table 3 and Figures 8, 9, S6, S7 illustrate a stark difference in EPR response: Electrochemical reduction produces single line signals near the free electron value of 2.0023 (Figures S6, S7). This and the observability at room temperature suggest an organic radical species with very little contribution from the metals to the spin distribution.[23,24] A small *g* anisotropy can be noted in the frozen state but there is no hyperfine splitting visible as may be possible under favourable circumstances.[16]

Oxidation produces EPR signals only at low temperatures in the frozen state with significant anisotropy of the *g* value. Axial $\mathbf{3}^+$ and rhombic splittings ($\mathbf{4}^+$–$\mathbf{6}^+$, Figures 8, 9) have been observed, and the amount of g_1-g_3 splitting in comparison[24] to other paramagnetic ruthenium complexes suggests major metal contributions to the spin distribution. The large spin orbit coupling[25] of the heavy element ruthenium is responsible for the *g* anisotropy and the rapid relaxation, allowing EPR signal observation only at low temperatures.[23,24] The different manifestations of *g* anisotropy in cations $\mathbf{3}^+$–$\mathbf{6}^+$ reflect the geometrical and electronic structures. Mononuclear $\mathbf{3}^+$ exhibits an axial *g* splitting (Figure 8, left) as befits a single low-spin d^5 ion Ru^{3+}. The corresponding dinuclear $\mathbf{4}^+$ shows a slight rhombic behaviour (Figure 8, right), corresponding to the approximately centrosymmetric arrangement. The mixed valence in $\mathbf{4}^+$ also results in rapid relaxation which leads to broad lines. Cations $\mathbf{5}^+$ and $\mathbf{6}^+$ are structurally similar and thus exhibit comparable EPR features (Table 3). The considerable *g* anisotropy Δg from a rhombic splitting (Figure 9) reflects the low symmetry resulting from the strongly π accepting tetrazine and less accepting pyrimidine ring. The Class II behaviour of the mixed-valent cations produces close-lying frontier MOs as evident from large Δg values.

UV/Vis/NIR Spectroelectrochemistry

Both the combination of electron rich Ru^{II} with π accepting tetrazine ligands and the reversible electron transfer reactions allowed us to study the metal complexes by UV/Vis/NIR spectroelectrochemistry, using an optically transparent thin-layer electrode (OTTLE) cell[26,27] (Figures 10–13, S8-S10, Table 4).

Table 3. X band EPR data[a] of electrochemically oxidized and reduced species.

compound	g_1	g_2	g_3	g_{iso}[b]	Δg[c]	compound	g
$\mathbf{3}^+$	2.213	2.196	1.900	2.103	0.313	$\mathbf{3}^{\bullet-}$[d]	1.992
$\mathbf{4}^+$	2.338	2.202	1.808	2.133	0.581	[e]	
$\mathbf{5}^+$	2.304	2.157	1.888	2.116	0.416	$\mathbf{5}^{\bullet-}$[d]	2.004
$\mathbf{6}^+$	2.302	2.159	1.885	2.115	0.417	$\mathbf{6}^{\bullet-}$[d]	2.007/1.996, $g_\perp/g_{\|\|}$

[a] Electrochemically generated species in CH_2Cl_2/0.1 M Bu_4NPF_6 at 120 K. [b] g_{iso} = isotropic $g = \sqrt{g_1^2 + g_2^2 + g_3^2/3}$. [c] $\Delta g = g_1 - g_3$. [d] Room temperature. [e] Not determined.

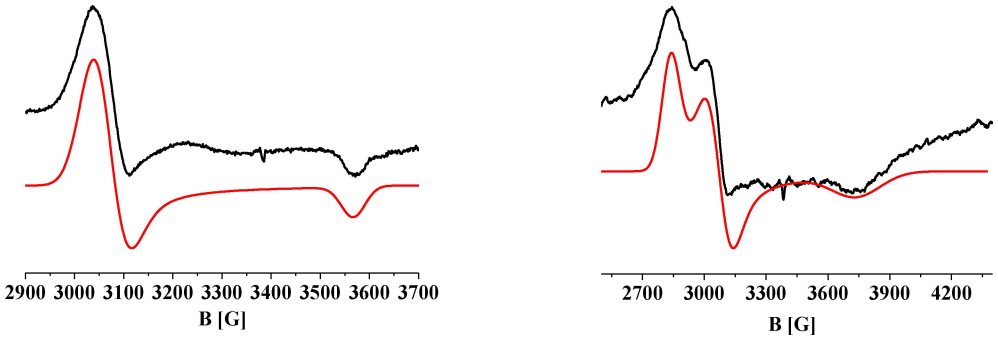

Figure 8. X band EPR spectra of $\mathbf{3}^+$ (left) and of $\mathbf{4}^+$ (right) in CH_2Cl_2/0.1 M Bu_4NPF_6 at 120 K with simulation (red line).

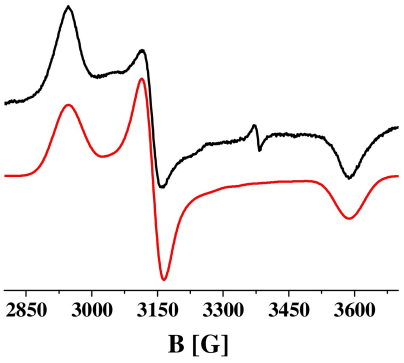

Figure 9. X band EPR spectrum of $\mathbf{6}^{+}$ in CH_2Cl_2/0.1 M Bu_4NPF_6 at 120 K and with simulation (red line), small impurity signal at $g \approx 2$.

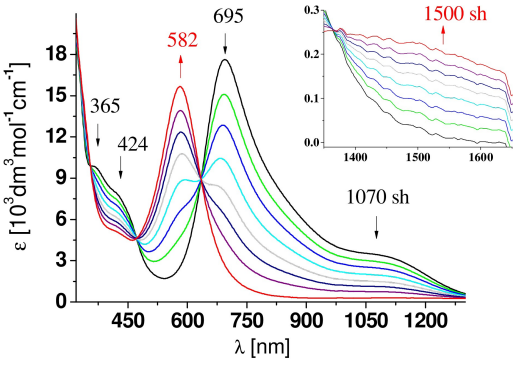

Figure 10. UV/Vis/NIR spectroelectrochemical response of the oxidation of $\mathbf{4} \rightarrow \mathbf{4}^{+}$ in CH_2Cl_2/0.1 M Bu_4NPF_6.

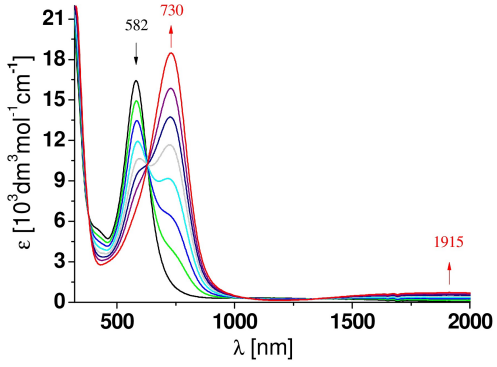

Figure 11. UV/Vis/NIR spectroelectrochemical response of the oxidation $\mathbf{4}^{+} \rightarrow \mathbf{4}^{2+}$ in CH_2Cl_2/0.1 M Bu_4NPF_6.

The dinuclear starting compounds **4**–**6** and the mononuclear complex **3** are distinguished by intense metal-to-ligand charge transfer (MLCT) absorptions in the visible ($\lambda_{max} = 500$–700 nm, involving the low-lying π* orbital of tetrazine as target (LUMO)). The occurrence of more than one band reflects the presence of other π acceptor heterocycles (pyridine, pyrimidine) in addition to the stronger π accepting tetrazine.[17]

Reduction to tetrazine radical anion complexes of ruthenium(II) produces rather small spectral changes.[23] The tetrazine anion radical components of the reduced ligands in the anionic complexes contribute to the rather limited shifts. The first one-electron oxidation to yield a mixed-valent (Ru^{III}-Ru^{II}) intermediate should produce an inter-valence charge transfer (IVCT) absorption at long wavelengths, typically in the near infrared (NIR) region.[9,10] However, such transitions are known to be very weak for tetrazine-bridged systems[11,13c,14] which is also noted here. Figure 10 shows the emergent weak shoulder around 1500 nm for $\mathbf{4}^{+}$, and even less observable features ($\varepsilon < 20\ M^{-1}cm^{-1}$) were found for $\mathbf{5}^{+}$ and $\mathbf{6}^{+}$ in the same spectral region (Table 4). The combination of very high K_c values and very weak IVCT absorptions is apparently[13c] a hallmark of tetrazine bridged Ru^{III}-Ru^{II} mixed-valent intermediates, its origin will have to be further investigated through quantum chemical calculations. This observation relates to the concept that electron-poor ligands are poor conduits for hole transfer.[24b,c,28] The dications resulting from second oxidation (Figures 11, 13) display intense bands from ligand-to ligand and ligand-to-metal charge transfer around 700 nm between the visible and near infrared regions (Figures 11, 13). Compound **4** is distinguished by a weak infrared absorption at 1915 nm after the second oxidation (Figure 11, Table 4). This transition is attributed to an LMCT (ligand-to-metal charge transfer) favoured by the presence of a donor substituted tetrazine bridge **1** and two oxidized metal centers. Redox systems $\mathbf{5}^{n+}$ and $\mathbf{6}^{n+}$ exhibit comparable spectra and spectral changes, as noted earlier for the very similar EPR response.

Conclusion

Three dinuclear ruthenium compounds have been synthesized and studied in 4 different oxidation states (−,0,+,2+). The neutral precursors (which may be reduced to radical complexes) contain π accepting tetrazine bridges and electron rich ruthenium(II) metals, without major intramolecular electron transfer, as confirmed structurally and spectroscopically. Structural analysis of one of the mixed-valent intermediates ($\mathbf{6}^{+}$) suggests a Class II situation according to the Robin/Day classification scheme.[22] As in other tetrazine ligand bridged examples,[11,12,14,18] the mixed-valent species are thermodynamically stable over an unusually large potential range, as quantified by comproportionation constants $10^{9.2} < K_c < 10^{14.1}$, but exhibit only very weak IVCT absorptions in the near IR region.

Supporting Information

The Supporting Information including the Experimental Section is available free of charge at https://doi.org/10.1002/zaac.202200152. CCDC-2160778, CCDC-2160779, CCDC-2160780, CCDC-2160781, CCDC-2160782, CCDC-2160783 and CCDC-2160784 contain the supplementary crystallographic data for this paper. These data can be obtained free of charge via www.

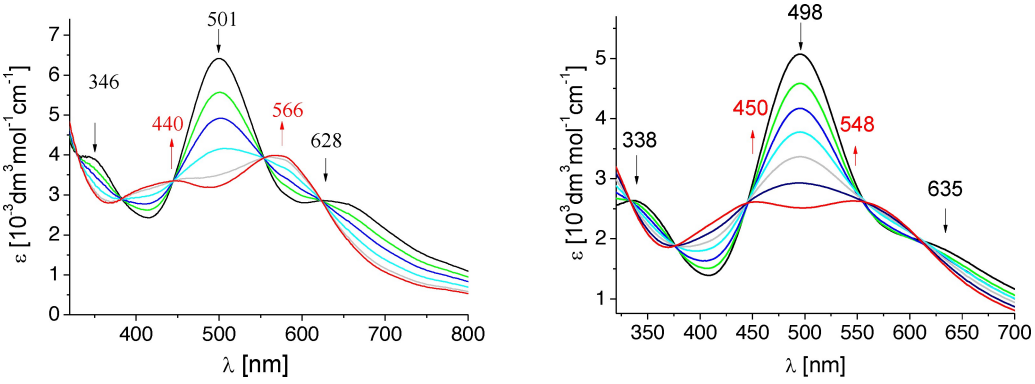

Figure 12. UV/Vis spectroelectrochemical response of the oxidation **5**→**5**$^{+}$ (left) and **6**→**6**$^{+}$ (right) in CH_2Cl_2/0.1 M Bu_4NPF_6.

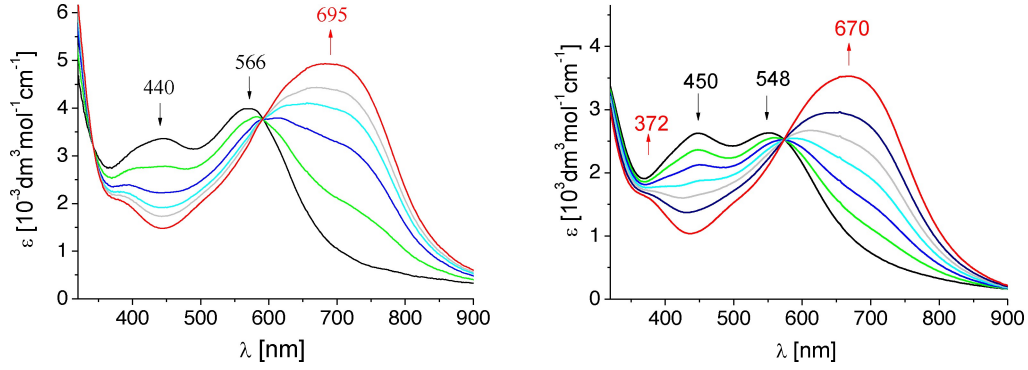

Figure 13. UV/Vis spectroelectrochemical response of the second oxidation **5**$^{+}$→**5**$^{2+}$ (left) and **6**$^{+}$→**6**$^{2+}$ (right) in CH_2Cl_2/0.1 M Bu_4NPF_6.

Table 4. Absorption data from UV/Vis/NIR spectroelectrochemistry.

complex	λ [nm] (ε [10^3 dm^3 mol^{-1} cm^{-1}])			
		reduction	oxidation	2nd oxidation
3	380 sh	428 (2.79)	449 (1.35)	
	512 (3.44)	563 (2.81)	572 (2.60)	
meso-**4**	365 (10.0)			
	424 sh	441 (12.12)		
	695 (17.61)	678 (11.02)	582 (16.41)	730 (18.40)
	1070 sh	1050 sh	1500 sh	1915 (0.66)
rac/meso-**5**	346 (4.11)	368 (6.19)		395 sh
	501 (6.34)	512 (6.10)	440 (3.35)	
	628 (2.90)	682 (3.85)	566 (4.00)	695 (4.95)
		730 sh	1500 sh	
rac/meso-**6**	338 (2.65)	415 (2.46)	320 sh	372 sh
	498 (5.11)	538 (3.93)	450 (2.65)	
	635 sh		548 (2.70)	670 (3.55)
	1061 (0.21)		1350 sh	

ccdc.cam.ac.uk/data_request/cif, or by emailing data_request@ccdc.cam.ac.uk, or by contacting The Cambridge Crystallographic Data Centre, 12 Union Road, Cambridge CB2 1EZ, UK; fax: +44 1223 336033.

Acknowledgements

The authors acknowledge support by the state of Baden-Württemberg. The contributions by Dipl.-Chem. Angela Winkelmann and Dr. Wolfgang Frey are gratefully acknowledged. J.F. thanks the Czech Science Foundation (project 19-03160S) for support. Open Access funding enabled and organized by Projekt DEAL.

Conflict of Interest

The authors declare no conflict of interest.

Data Availability Statement

The data that support the findings of this study are openly available in The Cambridge Crystallographic Data Centre, 12 Union Road, Cambridge CB2 1EZ, UK at www.ccdc.cam.ac.uk/data_request/cif, reference number 2160778.

Keywords: Crystal structure · Cyclic voltammetry · Diruthenium compounds · EPR spectroscopy · Spectroelectrochemistry

[1] T. M. Klapötke, A. Preimesser, J. Stierstorfer, *Z. Naturforsch.* **2013**, 68b, 1310–1326.
[2] H. Wu, N. K. Devaraj, *Acc. Chem. Res.* **2018**, 51, 1249–1259.
[3] a) O. Stetsiuk, A. Abhervé, N. Avarvari, *Dalton Trans.* **2020**, *49*, 5759–5777; b) F. Miomandre, P. Audebert, *J. Photochem: Photobiol C: Photochem. Rev.* **2020**, 44, 100372.
[4] W. Kaim, *Coord. Chem. Rev.* **2002**, 230, 127–139.
[5] M. Glöckle, W. Kaim, A. Klein, E. Roduner, G. Hübner, S. Zalis, J. van Slageren, F. Renz, P. Gütlich, *Inorg. Chem.* **2001**, 10, 2256–2262.
[6] M. Glöckle, K. Hübler, H.-J. Kümmerer, G. Denninger, W. Kaim, *Inorg. Chem.* **2001**, *40*, 2263–2269.
[7] W. Kaim, J. Fees, *Z. Naturforsch. B: Chem. Sci.* **1995**, *50*, 123–127.
[8] a) T. J. Woods, M. F. Ballesteros-Rivas, S. M. Ostrowsky, A. V. Palii, O. S. Reu, S. J. Klokishner, K. R. Dunbar, *Chem. Eur. J.* **2015**, *21*, 10302–10305; b) T. J. Woods, M. F. Ballesteros-Rivas, S. Gómez-Coca, E. Ruiz, K. R. Dunbar, *Inorg. Chem.* **2017**, *56*, 12094–12097.
[9] C. Creutz, *Prog. Inorg. Chem.* **1983**, *30*, 1–73.
[10] R. J. Crutchley, *Adv. Inorg. Chem.* **1994**, *41*, 273–325.
[11] S. Patra, B. Sarkar, S. Ghumaan, J. Fiedler, W. Kaim, G. K. Lahiri, *Inorg. Chem.* **2004**, 43, 6108–6113.
[12] S. Chellamma, M. Lieberman, *Inorg. Chem.* **2001**, 40, 3177–3180.
[13] a) B. Sarkar, S. Patra, J. Fiedler, R. Sunoj, D. Janardanan, S. M. Mobin, M. Niemeyer, G. K. Lahiri, W. Kaim, *Angew. Chem. Int. Ed.* **2005**, *44*, 5655–5658; *Angew. Chem.* **2005**, *117*, 5800–5803; b) B. Sarkar, S. Patra, J. Fiedler, R. B. Sunoj, D. Janardanan, G. K. Lahiri, W. Kaim, *J. Am. Chem. Soc.* **2008**, *130*, 3532–3542; c) W. Kaim, B. Sarkar, *Coord. Chem. Rev.* **2007**, *251*, 584–594.
[14] J. Poppe, M. Moscherosch, W. Kaim, *Inorg. Chem.* **1993**, 32, 2640–2643.
[15] S. Kohlmann, S. Ernst, W. Kaim, *Angew. Chem. Int. Ed. Engl.* **1985**, 24, 684–685.
[16] W. Kaim, S. Ernst, S. Kohlmann, P. Welkerling, *Chem. Phys. Lett.* **1985**, 118, 431–434.
[17] S. D. Ernst, W. Kaim, *Inorg. Chem.* **1989**, *28*, 1520–1528.
[18] S. Ernst, V. Kasack, W. Kaim, *Inorg. Chem.* **1988**, *27*, 1146–1148.
[19] a) B. Sarkar, S. Frantz, W. Kaim, C. Duboc, *Dalton Trans.* **2004**, 3727–3731; b) S. Patra, B. Sarkar, S. Ghumaan, M. P. Patil, S. M. Mobin, R. B. Sunoj, W. Kaim, G. K. Lahiri, *Dalton Trans.* **2005**, 1188–1194; c) A. Nayak, S. Patra, B. Sarkar, S. Ghumaan, V. G. Puranik, W. Kaim, G. K. Lahiri, *Polyhedron* **2005**, 24, 333–342.
[20] M. Schnierle, M. Leimkühler, M. R. Ringenberg, *Inorg. Chem.* **2021**, 60, 6367–6374.
[21] S. Patra, T. A. Miller, B. Sarkar, M. Niemeyer, M. D. Ward, G. K. Lahiri, *Inorg. Chem.* **2003**, 43, 4707–4713.
[22] M. B. Robin, P. Day, *Adv. Inorg. Chem. Radiochem.* **1968**, *10*, 247–422.
[23] W. Kaim, in *Electron Transfer in Chemistry*, V. Balzani, ed., Wiley-VCH (Weinheim), 2001, Vol. 2, pp 976–1002.
[24] a) E. Waldhör, B. Schwederski, W. Kaim, *J. Chem. Soc. Perkin Trans. 2* **1993**, 2109–2111; b) W. Kaim, G. K. Lahiri, *Angew. Chem. Int. Ed.* **2007**, *46*, 1778–1796; *Angew. Chem.* **2007**, *119*, 1808–1828; c) V. Kasack, W. Kaim, H. Binder, J. Jordanov, E. Roth, *Inorg. Chem.* **1995**, *34*, 1924–1933.
[25] J. A. Weil, J. R. Bolton, *Electron Paramagn. Reson.*, 2nd ed., Wiley, Hoboken, 2007.
[26] M. Krejčik, M. Danek, F. Hartl, *J. Electroanal. Chem. Interfacial Electrochem.* **1991**, 317, 179–187.
[27] W. Kaim, J. Fiedler, *Chem. Soc. Rev.* **2009**, *38*, 3373–3382.
[28] a) C. E. B. Evans, M. L. Naklicki, A. R. Rezvani, C. A. White, V. V. Kondratiev, R. J. Crutchley, *J. Am. Chem. Soc.* **1998**, *120*, 13096–13103; b) C. E. B. Evans, G. P. A. Yap, R. J. Crutchley, *Inorg. Chem.* **1998**, *37*, 6161–6167.

Manuscript received: April 13, 2022
Revised manuscript received: June 1, 2022
Accepted manuscript online: June 3, 2022

